

Supporting Information

Boosting the OER Activity of Amorphous IrO_x in Acidic Medium by Tuning its Electron Structure Using Lanthanum Salt Nanosheets

Xuefeng Wang,^a Haeseong Jang,^{b,d} Zijian Li,^c Haisen Li,^a Guangkai Li,^a Min Gyu Kim,^{b,*} Xuqiang Ji,^{a,e,*} Qing Qin,^{a,*} and Xien Liu^{a,*}

^aCollege of Chemical Engineering, Qingdao University of Science and Technology, Qingdao 266042, P. R. China. E-mail: xuqianglucky@163.com, qinqing@qust.edu.cn, liuxien@qust.edu.cn

^bBeamline Research Division, Pohang Accelerator Laboratory (PAL), Pohang 790-784 (Korea).
E-mail: mgkim@postech.ac.kr

^cDepartment of Chemistry, City University of Hong Kong, Hong Kong SAR, China

^dEnergy Storage and Distributed Resources Division, Lawrence Berkeley National Laboratory, Berkeley, California 94720, United States

^eCollege of Materials Science and Engineering, Qingdao University, Qingdao 266071, China

List of contents

1. Materials characterizations

2. Electrochemical measurement

Fig. S1 XRD pattern of the IrO_x/LaCO₃OH.

Fig. S2 SEM pattern of the amorphous IrO_x.

Fig. S3 XRD pattern of the Amorphous IrO_x.

Fig. S4 HAADF-STEM image of the Amorphous IrO_x and the corresponding elemental mappings of Ir, and O.

Fig. S5 XRD pattern of the LaCO₃OH.

Fig. S6. (a) The linear relationship between the velocity ratio of O₂/N₂ and its GC peak area ratio. (b) GC profiles of O₂ and N₂ for IrO_x/LaCO₃OH after 0 and 600 s electrolysis.

Fig. S7 Cyclic voltammograms recorded at various scan rates (10 ~ 120 mV s⁻¹) for determining the double layer capacitance: (a) IrO_x/LaCO₃OH, (b) Commercial IrO₂, (c) amorphous IrO_x.

Fig. S8 Nyquist plots of electrochemical impedance spectra (EIS) of the IrO_x/LaCO₃OH.

Fig. S9 The durability testing of the IrO_x/LaCO₃OH by the chronopotentiometry at a benchmark of 10 mA cm⁻².

Fig. S10 Cyclic voltammograms recorded at various scan rates (10 ~ 120 mV s⁻¹) for determining the double layer capacitance: (a) IrO_x/LaCO₃OH-3:1, (b) IrO_x/LaCO₃OH-4:1 and (c) The double-layer capacitances of catalysts prepared at different molar ratios.

Fig. S11 (a) Polarization curves and (b) Tafel slopes of catalysts prepared at different molar ratios.

Fig. S12 Cyclic voltammograms recorded at various scan rates (10 ~ 120 mV s⁻¹) for determining the double layer capacitance: (a) IrO_x/LaCO₃OH-160 °C and (b) The double-layer capacitances of catalysts prepared at different temperatures.

Fig. S13 (a) Polarization curves and (b) Tafel slopes of catalysts prepared at different temperatures.

Fig. S14 Cyclic voltammograms recorded at various scan rates (10 ~ 120 mV s⁻¹) for determining the double layer capacitance: (a) IrO_x/LaCO₃OH-12 h, (b) IrO_x/LaCO₃OH-36 h and (c) The double-layer capacitances of catalysts prepared at different reaction times.

Fig. S15 (a) Polarization curves and (b) Tafel slopes of catalysts prepared at different reaction times.

Fig. S16 SEM image of catalysts prepared with reaction for (a) 12 h and (b) 36 h.

Table S1 Comparison of the overpotentials at 10 mA cm^{-2} with recently reported OER catalysts in acidic media.

Materials characterizations

The morphology and composition of the materials were characterized by SEM, TEM, XRD, XPS, XANES and EXAFS measurements. The Rigaku diffraction system (D/Max2000) was used to record the XRD patterns of the prepared catalysts. The microstructures and morphology of catalysts were measured by the scanning electron microscope (Hitachi S-4800). The JEOL JEM-2100F transmission electron microscope was used to perform the TEM and HRTEM measurements. Thermo Scientific ESCALAB 250Xi X-ray photoelectron spectrometer was used to detect the electronic structure and chemical state of Ir and O elements in catalyst structure. The XANES of Ir L_{III}-edge and La L_{III}-edge were measured at room temperature by the BL10c beam line at the Pohang Light Source (PLS-II), Korea.

Electrochemical measurement

In a typical three-electrode system, the 0.1 M HClO₄ solution was used as the electrolyte. The working electrode was prepared by loading of 5 μL of the catalyst ink on a glassy carbon (GC: 3 mm in diameter). Carbon rod and Ag/AgCl were used as counter and reference electrodes, respectively. The working electrode was prepared according to the steps below: First, the prepared catalyst powder (2 mg) was added into 100 μL of deionized water and 200 μL ethanol with 40 μL of 5 wt % Nafion solution. Next, 1mg of carbon black (XC-72) was added to the formulated ink. The polarization curves were measured in the potential range of 1.20 V to 1.70 V (vs RHE) and the scanning speed was 5 mV s⁻¹. All data were compensated with iR (95%). ESI measurements were made at an open circuit potential in the frequency range of 100 kHz to 0.1 Hz. The durability testing was performed by a chronopotentiometry method at a current density of 10 mA cm⁻². The activity and stability of commercially available IrO₂ (Macklin, 99.9%) for OER was determined under the same condition.

Measurement of the Faraday Efficiency: A piece of Ti mesh coated by 1 mg IrO_x/LaCO₃OH (surface area = 1 cm²) was used as the working electrode. Before measurement, the cell was purged by N₂ gas for about 20 min to to detect the air tightness of the cell. A linear relationship between the O₂ and N₂ gas flow rate and its GC peak area ratio was obtained by plotting five GC measurements of adjust flow rate O₂ samples with fixed flow rate of N₂ is 5 sccm. The GC measurements were measured by FULI INSTRUMENTS GC 9790 plus gas chromatograph.

The GC peak area has a relationship: $A(\text{oxygen product}) = [A(\text{oxygen } 600 \text{ s}) - A(\text{oxygen } 0 \text{ s})]$, as shown in Fig. S6. Therefore, $A(\text{N}_2/\text{O}_2) = A(\text{nitrogen } 600\text{s})/A[(\text{oxygen } 600\text{s}) - A(\text{oxygen } 0\text{s})] = 4518290/[88888.4 - 29650.8] = 76.27$. Take this ratio into the linear equation. O_2 flow rate = $5/[1.965 \times 76.27 - 0.36899] = 0.03345$ sccm. The product amount is $n_{\text{O}_2} = 0.03345 \times 10 \times 10^{-3} / 22.45 = 1.49 \mu\text{mol}$. After 600s, amount of charge transferred by reaction were 6.0189C. The ideal product amount is $n(\text{O}_2, \text{theoretical}) = C/F/4 = 6.0189/(96485 \times 4) = 1.56 \mu\text{mol}$, where C is the amount of charge transferred, F is the faraday constant (96485 C mol^{-1}). Therefore, the Faraday efficiency is $n(\text{O}_2, \text{experimental})/n(\text{O}_2, \text{theoretical}) \times 100\% = 1.49/1.56 \times 100\% = 95.5\%$.

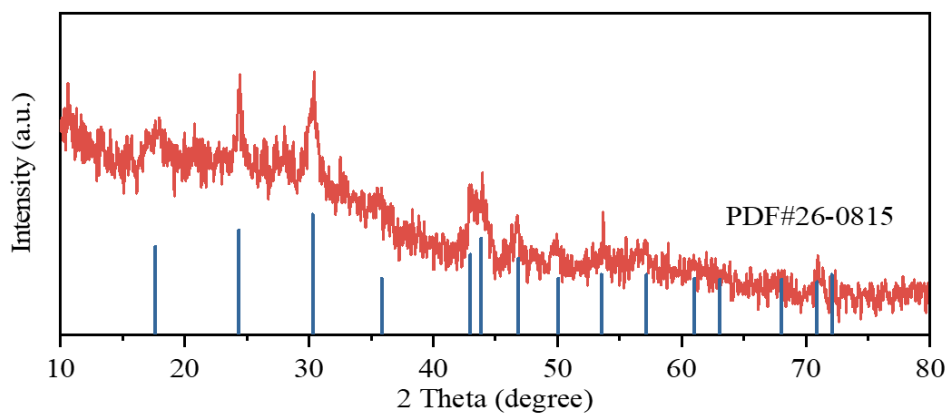


Fig. S1 The XRD pattern of the IrO_x/LaCO₃OH.

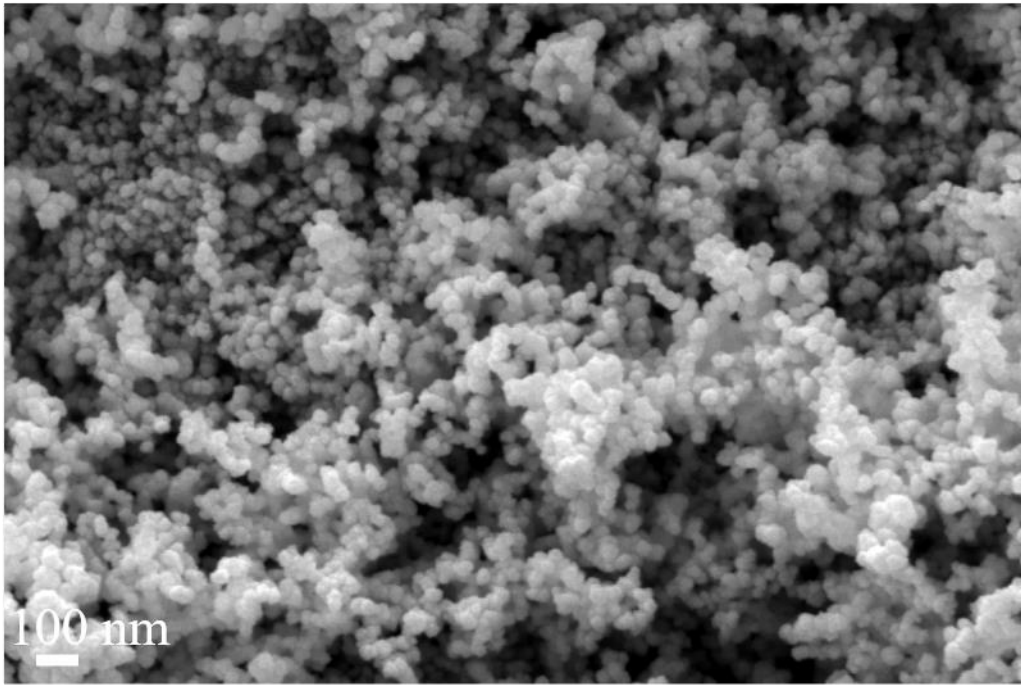


Fig. S2 The SEM pattern of the amorphous IrO_x.

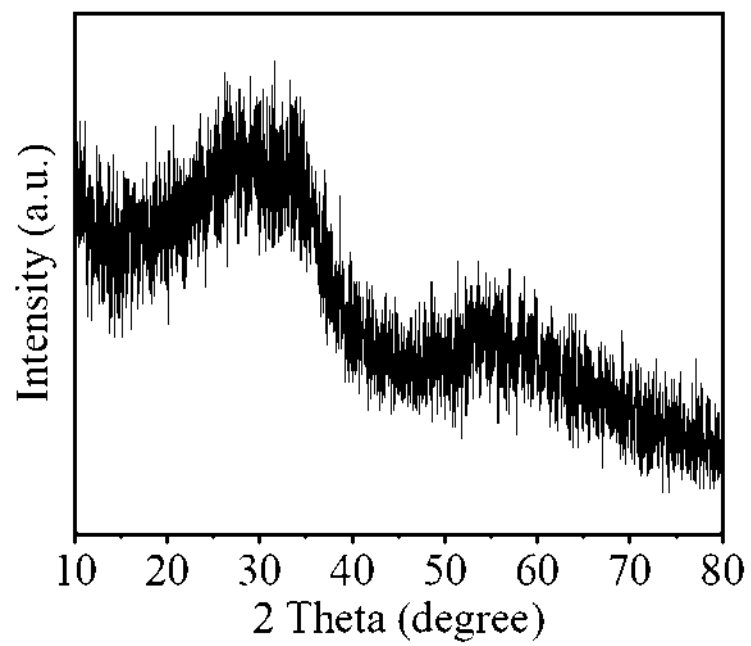


Fig. S3 The XRD pattern of the Amorphous IrO_x.

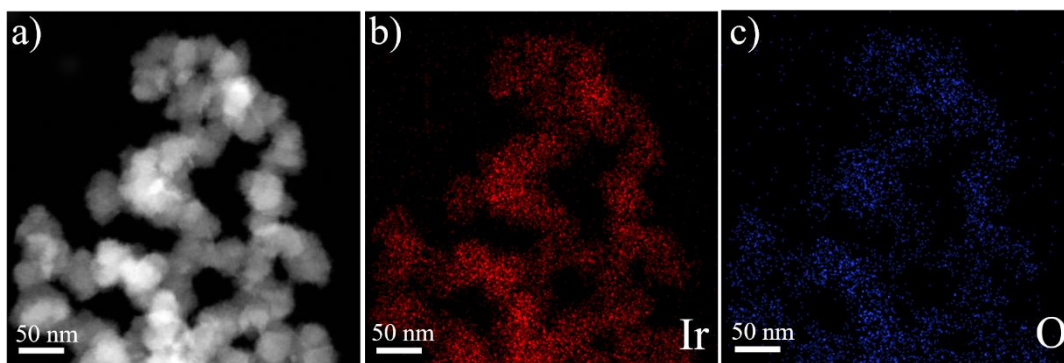


Fig. S4 HAADF-STEM image of the Amorphous IrO_x and the corresponding elemental mappings of Ir, and O.

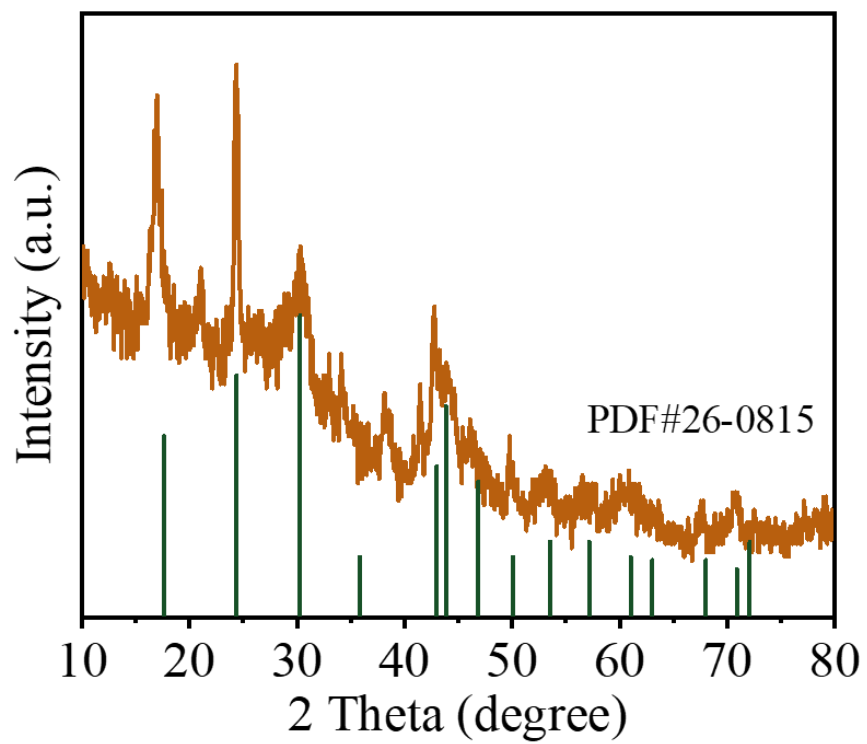


Fig. S5 The XRD pattern of the LaCO₃OH.

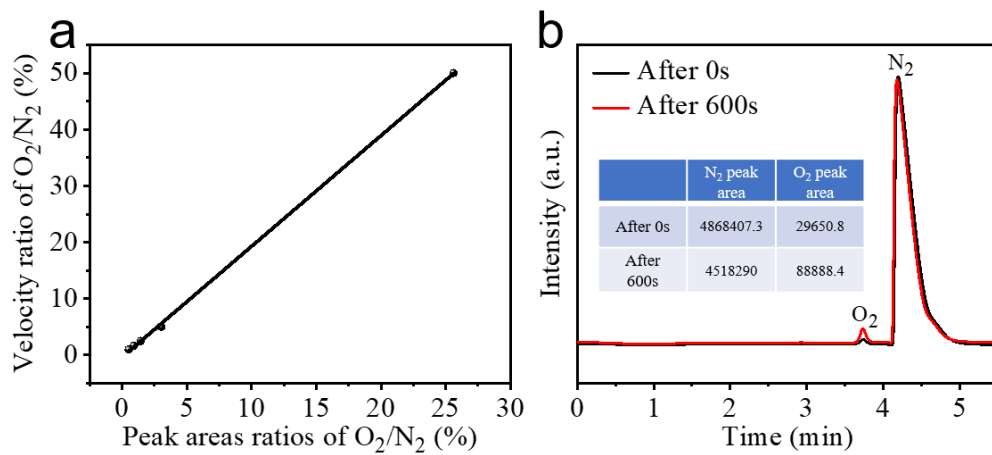


Fig. S6. (a) The linear relationship between the velocity ratio of O_2/N_2 and its GC peak area ratio. (b) GC profiles of O_2 and N_2 for $IrO_x/LaCO_3OH$ after 0 and 600 s electrolysis.

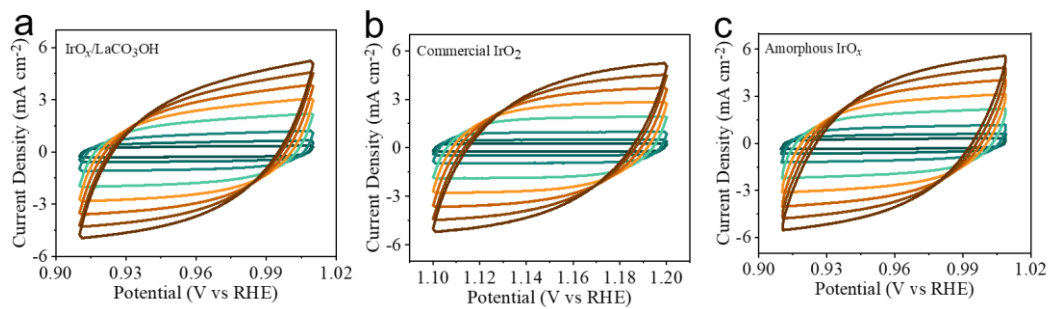


Fig. S7 Cyclic voltammograms recorded at various scan rates (10 ~ 120 mV s⁻¹) for determining the double layer capacitance: (a) IrO_x/LaCO₃OH, (b) Commercial IrO₂, (c) Amorphous IrO_x.

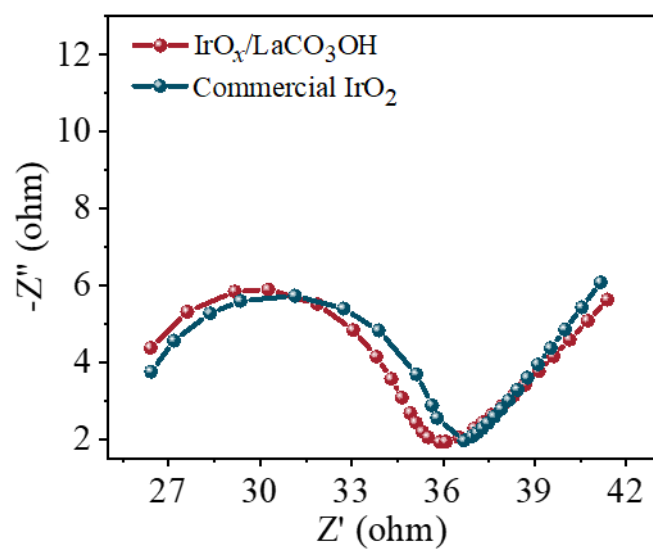


Fig. S8 Nyquist plots of electrochemical impedance spectra (EIS) of the IrO_x/LaCO₃OH.

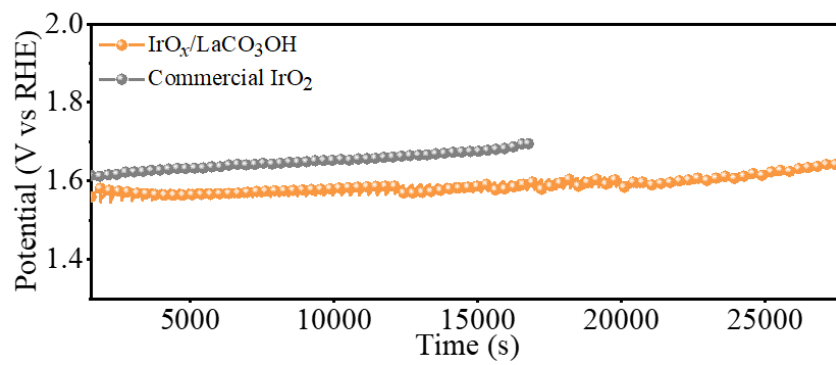


Fig. S9 Long-term chrono potentiometric curves of IrO_x/LaCO₃OH and Commercial IrO₂ at 10 mA cm⁻².

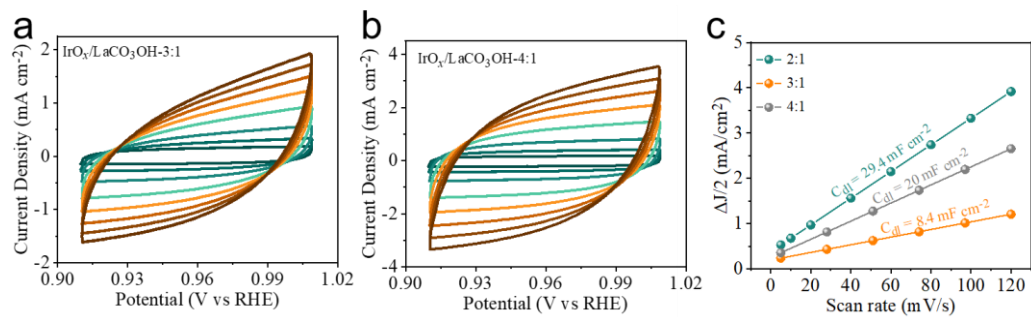


Fig. S10 Cyclic voltammograms recorded at various scan rates (10 ~ 120 mV s⁻¹) for determining the double layer capacitance: (a) IrO_x/LaCO₃OH-3:1, (b) IrO_x/LaCO₃OH-4:1 and (c) The double-layer capacitances of catalysts prepared at different molar ratios.

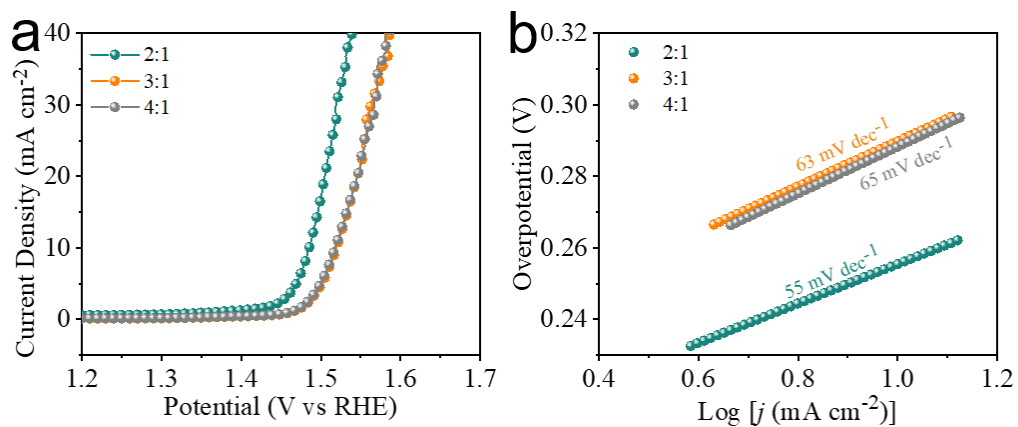


Fig. S11 (a) Polarization curves and (b) Tafel slopes of catalysts prepared at different molar ratios.

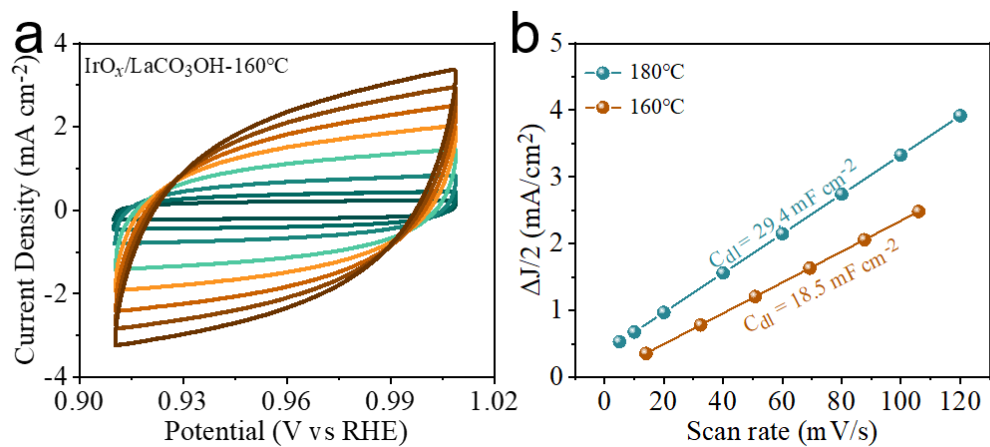


Fig. S12 Cyclic voltammograms recorded at various scan rates (10 ~ 120 mV s⁻¹) for determining the double layer capacitance: (a) IrO_x/LaCO₃OH-160°C and (b) The double-layer capacitances of catalysts prepared at different temperatures.

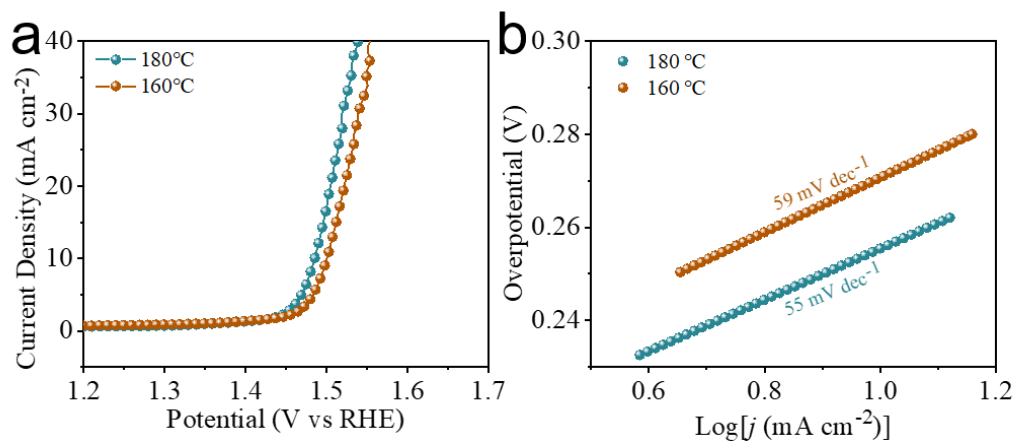


Fig. S13 (a) Polarization curves and (b) Tafel slopes of catalysts prepared at different temperatures.

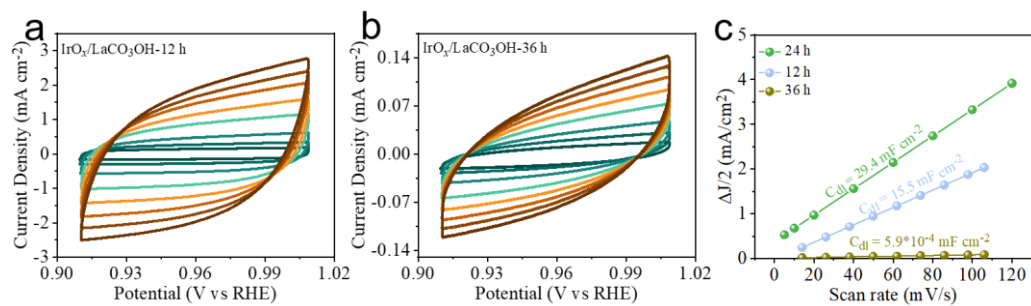


Fig. S14 Cyclic voltammograms recorded at various scan rates (10 ~ 120 mV s⁻¹) for determining the double layer capacitance: (a) IrO_x/LaCO₃OH-12 h, (b) IrO_x/LaCO₃OH-36 h and (c) The double-layer capacitances of catalysts prepared at different reaction times.

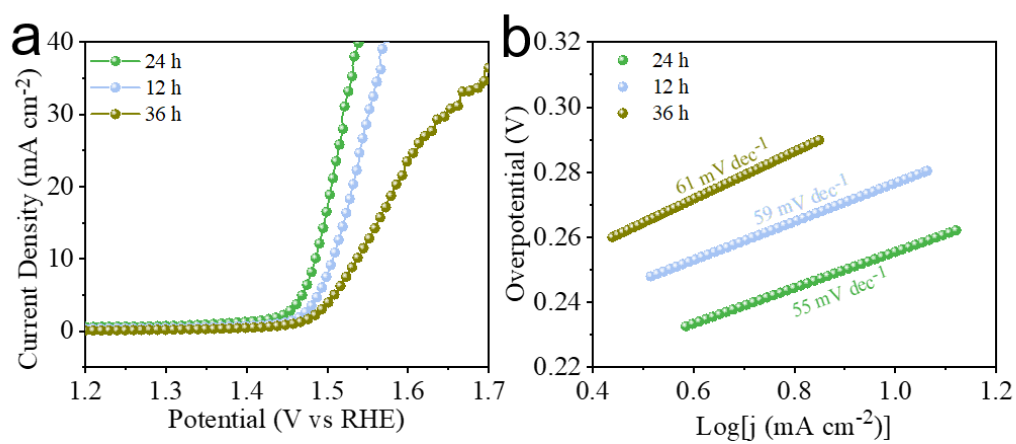


Fig. S15 (a) Polarization curves and (b) Tafel slopes of catalysts prepared at different reaction times.

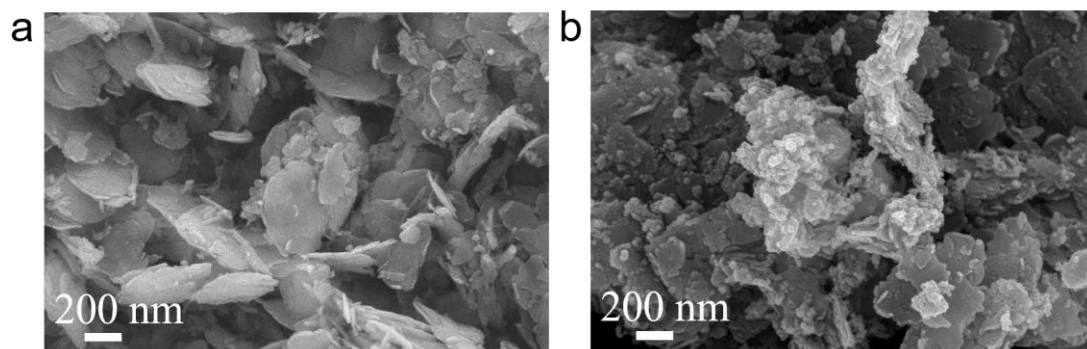


Fig. S16. SEM image of catalysts prepared with reaction for (a) 12 h and (b) 36 h.

Table S1 Comparison of the overpotentials at 10 mA cm^{-2} with recently reported OER catalysts in acidic media

Electrocatalyst	Electrolyte	Overpotential(mV)	References
		at 10 mA cm^{-2}	
Commercial RuO ₂	0.1 M HClO ₄	315	This work
IrO _x /LaCO ₃ OH	0.1 M HClO ₄	255	This work
NiIrRuAl-1/3	0.1 M HClO ₄	237	[1]
6H-SrIrO ₃	0.5 M H ₂ SO ₄	248	[2]
La-Ir NF	0.1 M HClO ₄	263	[3]
SrIrO-1100	0.5 M H ₂ SO ₄	263	[4]
RuCu	0.5 M H ₂ SO ₄	270	[5]
IrCuNi DCNCs	0.1 M HClO ₄	273	[6]
Ni _{0.34} Co _{0.46} Ir _{0.2} O ₆	0.1 M HClO ₄	280	[7]
IrCo	0.5 M H ₂ SO ₄	284	[8]
Ir _{0.4} Mn _{0.6} O ₆	0.1 M H ₂ SO ₄	285	[9]
Sr ₂ IrO ₄	0.1 M HClO ₄	286	[10]
La ₃ IrO ₇ -SLD	0.1 M HClO ₄	296	[11]
Ir _{0.06} Co _{2.94} O ₄	0.1 M HClO ₄	300	[12]
IrO _x -03	0.1 M HClO ₄	300	[13]
IrO _x /Pr ₃ IrO ₇	0.1 M HClO ₄	305	[14]
IrNiO _x TF	0.1 M HClO ₄	315	[15]
Ir/C ₀₄ N	0.5 M H ₂ SO ₄	319	[16]

0.5IrO₂-0.5SiO₂	0.5 M H ₂ SO ₄	322	[17]
IrNi/NiOHT	0.1 M HClO ₄	329	[18]
Ir_{0.7}Co_{0.3}O_x	0.5 M H ₂ SO ₄	330	[19]
IrNiO_x	0.1 M HClO ₄	332	[18]
Ir HT	0.1 M HClO ₄	336	[18]
Ir_{0.3}Mo_{0.7}O₆	0.1 M HClO ₄	345	[20]
Ir/Ni₄N	0.5 M H ₂ SO ₄	346	[16]
Ba₂YIrO₆	0.1 M HClO ₄	350	[21]
K_{x=0.25}IrO₂	0.1 M HClO ₄	350	[22]
SrIrO₃	0.1 M HClO ₄	353	[10]
Bi₂Ir₂O₇	1 M H ₂ SO ₄	365	[23]
RuIrCoO_x	0.5 M H ₂ SO ₄	394	[24]

References

- [1] N. Liu, K. Yin, C. Si, T. Kou, Y. Zhang, W. Ma, Z. Zhang, Hierarchically porous nickel–iridium–ruthenium–aluminum alloys with tunable compositions and electrocatalytic activities towards the oxygen/hydrogen evolution reaction in acid electrolyte, *J. Mater. Chem. A.*, 2020, **8**, 6245-6255.
- [2] L. Yang, G. Yu, X. Ai, W. Yan, H. Duan, W. Chen, X. Li, T. Wang, C. Zhang, X. Huang, J.S. Chen, X. Zou, Efficient oxygen evolution electrocatalysis in acid by a perovskite with face-sharing IrO₆ octahedral dimers, *Nat. Commun.*, 2018, **9**, 5236.
- [3] W. Sun, C. Ma, X. Tian, J. Liao, J. Yang, C. Ge, W. Huang, An amorphous lanthanum–iridium solid solution with an open structure for efficient water splitting, *J. Mater. Chem. A.*, 2020, **8**, 12518-12525.
- [4] L. Zhang, H. Jang, Z. Li, H. Liu, M. G. Kim, X. Liu, J. Cho, SrIrO₃ modified with laminar Sr₂IrO₄ as a robust bifunctional electrocatalyst for overall water splitting in acidic media, *Chem. Eng. J.*, 2021, **419**, 129604.
- [5] Y. Li, W. Zhou, X. Zhao, W. Cheng, H. Su, H. Zhang, M. Liu, Q. Liu, Donutlike RuCu Nanoalloy with Ultrahigh Mass Activity for Efficient and Robust Oxygen Evolution in Acid Solution, *ACS Appl. Energy Mater.*, 2019, **2**, 7483-7489.
- [6] D. Liu, Q. Lv, S. Lu, J. Fang, Y. Zhang, X. Wang, Y. Xue, W. Zhu, Z. Zhuang, IrCuNi Deeply Concave Nanocubes as Highly Active Oxygen Evolution Reaction Electrocatalyst in Acid Electrolyte, *Nano Lett.*, 2021, **21**, 2809-2816.
- [7] W. Q. Zaman, W. Sun, M. Tariq, Z. Zhou, U. Farooq, Z. Abbas, L. Cao, J. Yang,

Iridium substitution in nickel cobaltite renders high mass specific OER activity and durability in acidic media, *Appl. Catal. B*, 2019, **244**, 295-302.

- [8] J. Zhu, M. Wei, Q. Meng, Z. Chen, Y. Fan, S. W. Hasan, X. Zhang, D. Lyu, Z. Q. Tian, P. K. Shen, Ultrathin-shell IrCo hollow nanospheres as highly efficient electrocatalysts towards the oxygen evolution reaction in acidic media, *Nanoscale.*, 2020, **12**, 24070-24078.
- [9] Z. Zhou, W. Q. Zaman, W. Sun, L. M. Cao, M. Tariq, J. Yang, Cultivating crystal lattice distortion in IrO₂ via coupling with MnO₂ to boost the oxygen evolution reaction with high intrinsic activity, *Chem Commun.*, 2018, **54**, 4959-4962.
- [10] A. L. Strickler, D. Higgins, T. F. Jaramillo, Crystalline Strontium Iridate Particle Catalysts for Enhanced Oxygen Evolution in Acid, *ACS Appl. Energy Mater.*, 2019, **2**, 5490-5498.
- [11] Q. Qin, H. Jang, Y. Wang, L. Zhang, Z. Li, M. G. Kim, S. Liu, X. Liu, J. Cho, Getting La Effect from La₃IrO₇ as a Highly Efficient Electrocatalyst for Oxygen Evolution Reaction in Acid Media, *Adv. Energy Mater.*, 2020, **11**, 2003561.
- [12] J. Shan, C. Ye, S. Chen, T. Sun, Y. Jiao, L. Liu, C. Zhu, L. Song, Y. Han, M. Jaroniec, Y. Zhu, Y. Zheng, S. Z. Qiao, Short-Range Ordered Iridium Single Atoms Integrated into Cobalt Oxide Spinel Structure for Highly Efficient Electrocatalytic Water Oxidation, *J. Am. Chem. Soc.*, 2021, **143**, 5201-5211.
- [13] R. Sharma, M. A. Karlsen, P. Morgen, J. Chamier, D. B. Ravnsbæk, S. M. Andersen, Crystalline Disorder, Surface Chemistry, and Their Effects on the

Oxygen Evolution Reaction (OER) Activity of Mass-Produced Nanostructured Iridium Oxides, *ACS Appl. Energy Mater.*, 2021, **4**, 2552-2562.

- [14] Y. Wang, S. Liu, Q. Qin, H. Liu, L. Zhang, T. Wei, H. Li, X. Liu, Praseodymium iridium oxide as a competitive electrocatalyst for oxygen evolution reaction in acid media, *Sci. China Mater.*, 2021, **64**, 2193-2201.
- [15] T. Reier, Z. Pawolek, S. Cherevko, M. Bruns, T. Jones, D. Teschner, S. Selve, A. Bergmann, H.N. Nong, R. Schlogl, K.J. Mayrhofer, P. Strasser, Molecular Insight in Structure and Activity of Highly Efficient, Low-Ir Ir-Ni Oxide Catalysts for Electrochemical Water Splitting (OER), *J. Am. Chem. Soc.*, 2015, **137**, 13031-13040.
- [16] B. M. Tackett, W. Sheng, S. Kattel, S. Yao, B. Yan, K. A. Kuttiyiel, Q. Wu, J.G. Chen, Reducing Iridium Loading in Oxygen Evolution Reaction Electrocatalysts Using Core–Shell Particles with Nitride Cores, *ACS Catal.*, 2018, **8**, 2615-2621.
- [17] J. J. Zhang, J. M. Hu, J. Q. Zhang, C. N. Cao, IrO₂–SiO₂ binary oxide films: Geometric or kinetic interpretation of the improved electrocatalytic activity for the oxygen evolution reaction, *Int. J. of Hydrogen Energ.*, 2011, **36**, 5218-5226.
- [18] C. Spöri, P. Briois, H. N. Nong, T. Reier, A. Billard, S. Köhl, D. Teschner, P. Strasser, Experimental Activity Descriptors for Iridium-Based Catalysts for the Electrochemical Oxygen Evolution Reaction (OER), *ACS Catal.*, 2019, **9**, 6653-6663.
- [19] W. Hu, H. Zhong, W. Liang, S. Chen, Ir-Surface enriched porous Ir-Co oxide hierarchical architecture for high performance water oxidation in acidic media,

ACS Appl. Mater Inter., 2014, **6**, 12729-12736.

- [20] M. Tariq, W.Q. Zaman, W. Sun, Z. Zhou, Y. Wu, L.-m. Cao, J. Yang, Unraveling the Beneficial Electrochemistry of IrO₂/MoO₃ Hybrid as a Highly Stable and Efficient Oxygen Evolution Reaction Catalyst, *ACS Sustainable Chem. Eng.*, 2018, **6**, 4854-4862.
- [21] O. Diaz-Morales, S. Raaijman, R. Kortlever, P. J. Kooyman, T. Wezendonk, J. Gascon, W. T. Fu, M. T. Koper, Iridium-based double perovskites for efficient water oxidation in acid media, *Nat. Commun.*, 2016, **7**, 12363.
- [22] W. Sun, Y. Song, X. Q. Gong, L. M. Cao, J. Yang, Hollandite Structure K(x approximately 0.25)IrO₂ Catalyst with Highly Efficient Oxygen Evolution Reaction, *ACS Appl. Mater Inter.*, 2016, **8**, 820-826.
- [23] K. Sardar, S.C. Ball, J. D. B. Sharman, D. Thompsett, J. M. Fisher, R. A. P. Smith, P. K. Biswas, M. R. Lees, R. J. Kashtiban, J. Sloan, R. I. Walton, Bismuth Iridium Oxide Oxygen Evolution Catalyst from Hydrothermal Synthesis, *Chem. Mater.*, 2012, **24**, 4192-4200.
- [24] J. L. Corona-Guinto, L. Cardeño-García, D. C. Martínez-Casillas, J. M. Sandoval-Pineda, P. Tamayo-Meza, R. Silva-Casarin, R. G. González-Huerta, Performance of a PEM electrolyzer using RuIrCoO_x electrocatalysts for the oxygen evolution electrode, *Int. J. Hydrogen Energ.*, 2013, **38**, 12667-12673.